IEEE Access
Multidisciplinary | Rapid Review | Open Access Journal

Received February 3, 2021, accepted February 14, 2021, date of publication February 22, 2021, date of current version March 2, 2021.

Digital Object Identifier 10.1109/ACCESS.2021.3060774

Phase Inductance and Rotor Position Estimation for Sensorless Permanent Magnet Synchronous Machine Drives at Standstill

HAO-CHIEH YEH AND SHENG-MING YANG, (Member, IEEE)
Department of Electrical Engineering, National Taipei University of Technology, Taipei 10608, Taiwan
Corresponding author: Sheng-Ming Yang (smyang@ntut.edu.tw)

ABSTRACT Sensorless control is a common control method used in variable speed drive applications with permanent magnet synchronous machines (PMSMs). In these drive systems, phase inductance (i.e., q - and d -axis inductance) is the key parameter in designing current controllers. Additionally, the rotor position is essential for coordinate transformation during the motor startup. This paper presents the two offline methods of 1) line-to-line voltage injection and 2) stator qd voltage injection of sensorless PMSM drives for the estimation of phase inductance and initial rotor position, respectively. A distinct feature of the proposed methods is that they estimate both inductance and rotor position using the same algorithm. These methods were experimentally verified using an interior PMSM (IPMSM) and a surface-mounted PMSM (SPMSM). Because of the use of a least-squares algorithm, only a limited number of voltage vectors are required to achieve reasonable accuracy for measuring inductance. However, the accuracy of the estimated position was linearly proportional with the number of voltage vectors injected. Furthermore, the position error for IPMSM was found to be smaller than that for SPMSM.

INDEX TERMS Inductance estimation, least-square estimation, rotor initial position detection, resistance estimation, sensorless control.

I. INTRODUCTION

Permanent magnet synchronous machines (PMSMs) have wide industrial applications because of their high power and torque density. Vector control, which involves controlling the motor currents in a frame rotating synchronously with the rotor, is a typically used control method in PMSM drive systems. Electric parameters such as phase resistance and inductance are required for current controller design, and rotor position is essential for achieving coordinate transformation in the controller. Some PMSM drive systems are equipped with encoders or Hall sensors for determining the rotor position. However, in many applications, position sensors are impractical. For example, they are too expensive for low-cost applications, such as fans, and might be damaged by the refrigerants used in air conditioner compressors. Therefore, sensorless control algorithms have been developed for these applications [1]–[3].

Many offline methods have been developed for phase inductance measurement [4]–[11], some of which [4]–[6], [9] require aligning a rotor or locking it at several positions; other methods require a shaft position sensor [7], [8], [10], [11]. These requirements are mainly for identifying the positions of the q and d axes. Furthermore, locking a rotor can eliminate the rotor vibration during inductance measurement. In some applications, separating the motor from its mechanical load is extremely difficult, and thus, the methods proposed in [4]–[6] and [9] may be unsuited to these applications. Moreover, in applications without position sensors, the methods proposed in [7], [8], [10], and [11] cannot be used.

The limitations highlighted in [4]–[11] can be overcome using the initial position detection techniques proposed in [12]–[20]. The main principle behind standstill initial position detection for PMSMs is the use of the saliency effect. The secondary saliency harmonic effect was discussed in [12] and [13]; in particular, rotating voltage vector carrier signal injection was used for position and polarity detection in [12]. In addition, a two-step position estimation method was proposed to minimize the influence of secondary saliency harmonics on saliency-based drive [13], where polarity was obtained through voltage pulse signal injection at the estimated d axis. A high-frequency (HF) current signal extracted

The associate editor coordinating the review of this manuscript and approving it for publication was Ton Duc Do.

through a bandpass filter was used to obtain the rotor position [14], where voltage pulses were injected at the estimated d axis for polarity identification. In [15] and [16], the current control and voltage injection periods were separated to eliminate the requirement of a HF signal extraction filter. The rotor position was estimated during the voltage injection period, and polarity was detected by voltage injection at the estimated d axis. In addition, a recursive discrete Fourier transform [17] was applied to detect the rotor position and polarity; however, this method was highly computationally expensive. To address this problem, two fixed HF square-wave voltage signal injections [18] were used to estimate the rotor position, where the voltage signals were randomly injected into the estimated d axis. Polarity identification was completed by examining the accumulated induced random HF current peak pairs. A position detection method, involving three steps, was proposed in [19]. In that study, a voltage equation was first applied to a stationary frame to detect the approximate rotor position. Subsequently, voltage pulses were injected at the estimated d axis to determine the polarity, and finally, symmetric voltage pulses were injected for accurate position detection. In [20], voltage and current signals were injected to estimate the initial rotor position. The injected voltage pulses were HF square-wave signals, whereas the injected current signals were low-frequency (LF) sinusoidal signals; both signals were injected at the estimated d axis. A LF current signal was used to enhance the magnetic saturation effect, and the small current signals induced from the HF square-wave voltage were accumulated for polarity identification. In summary, injecting voltage pulses at the estimated d axis is a predominant method for polarity detection.

In combination with the initial position detection methods, inductance can be measured in shaft position applications without sensors [21]–[23]. In [21], the initial rotor position was determined by first using an HF injection method. Subsequently, inductance was obtained by applying voltage pulses at the estimated q and d axes. After the initial position detection, phase inductance was estimated through voltage pulses at the estimated q and d axes [22]. By using the initial position detection method proposed in [14], the authors in [23] applied a sinusoidal voltage to the estimated q and d axes and calculated the phase inductance by using the frequency response. The use of the two algorithms in these methods to separately estimate inductance and rotor position is a common approach, with rotor position required for inductance estimation.

Inductance exhibits saturation and crosscoupling effects [6]. The actual inductance does not remain constant during motor operations. However, if the variation in inductance is small enough, a common constant proportional–integral (PI) current controller can drive a PMSM with satisfactory response [11]. For large variations in inductance, the saturation and crosscoupling effects can be ignored in the current controller design when applying techniques such as a robust controller [24] or an online adaptive tuning algorithm [25]–[29]. For example, a robust current controller can tolerate 50% variation in inductance [24], and an online tuning controller [25] can achieve a deadbeat response even with >50% variation in nominal inductance. Thus, compensating for the saturation and crosscoupling effects in current controller design is unnecessary.

This paper proposes two offline methods for rapid phase inductance and initial rotor position estimation for sensorless PMSM drives: line-to-line voltage injection (LLVI), which is suitable for nonvector-controlled drives, and stator qd voltage injection (QDVI), which is suitable for vector-controlled drives. Both methods involve voltage vector injection and the use of a least-squares algorithm. A distinct feature of these methods is that they can estimate both inductance and rotor positions by using the same algorithm; furthermore, information on rotor position is not required for inductance estimation. After detecting the rotor position, phase resistance can be identified. The proposed methods are simpler to implement, more accurate, and more rapidly executed than most existing methods. The rest of this paper is organized as follows. Section 2 describes the mathematical model proposed for a PMSM. Section 3 presents both the principle underlying manual measurement using an LCR meter and an improved method for rotor position estimation. Sections 4 and 5 introduce the LLVI and stator QDVI methods, respectively, for sensorless drives. The method of identifying phase resistance is also explained in Section 5. Section 6 describes the experimental setup and results. Section 7 summarizes the conclusions.

II. MATHEMATICAL MODEL FOR PMSM

Fig. 1 illustrates the coordinate system used in this paper. The superscripts s and r denote the stator and rotor frames, respectively. The motor phase voltages can be expressed per [30] as follows:

$$\begin{bmatrix} v_{as} \\ v_{bs} \\ v_{cs} \end{bmatrix} = r_s \begin{bmatrix} i_{as} \\ i_{bs} \\ i_{cs} \end{bmatrix} + p \begin{bmatrix} \lambda_{as} \\ \lambda_{bs} \\ \lambda_{cs} \end{bmatrix} \tag{1}$$

$$\begin{bmatrix} \lambda_{as} \\ \lambda_{bs} \\ \lambda_{cs} \end{bmatrix} = \begin{bmatrix} L_{as,as} & L_{as,bs} & L_{as,cs} \\ L_{bs,as} & L_{bs,bs} & L_{bs,cs} \\ L_{cs,as} & L_{cs,bs} & L_{cs,cs} \end{bmatrix} \begin{bmatrix} i_{as} \\ i_{bs} \\ i_{cs} \end{bmatrix} + \begin{bmatrix} \lambda \sin(\theta_r) \\ \lambda \sin(\theta_r - 2\pi/3) \\ \lambda \sin(\theta_r + 2\pi/3) \end{bmatrix} \tag{2}$$

$$\begin{cases} L_{as,as} = L_{ls} + L_{0s} + L_{2s}\cos(2\theta_r) \\ L_{bs,bs} = L_{ls} + L_{0s} + L_{2s}\cos(2\theta_r + 2\pi/3) \\ L_{cs,cs} = L_{ls} + L_{0s} + L_{2s}\cos(2\theta_r - 2\pi/3) \end{cases} \tag{3}$$

$$\begin{cases} L_{as,bs} = L_{bs,as} = -0.5L_{0s} + L_{2s}\cos(2\theta_r - 2\pi/3) \\ L_{bs,cs} = L_{cs,bs} = -0.5L_{0s} + L_{2s}\cos(2\theta_r) \\ L_{cs,as} = L_{as,cs} = -0.5L_{0s} + L_{2s}\cos(2\theta_r + 2\pi/3) \end{cases} \tag{4}$$

where v_{as}, v_{bs}, and v_{cs} indicate the voltages in the three phases; i_{as}, i_{bs}, and i_{cs} are the currents in the three phases; p is

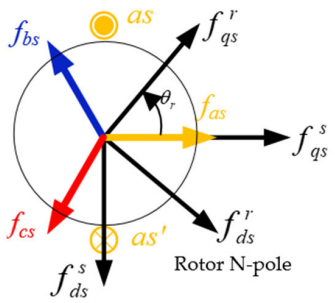

FIGURE 1. Coordinate system.

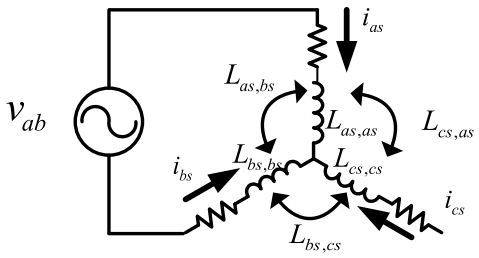

FIGURE 2. Manual inductance measurement setup.

the differential operator; λ is the flux linkage of the permanent magnets; θ_r is the rotor's electrical position; $L_{as,as}$, $L_{bs,bs}$, and $L_{cs,cs}$ indicate self-inductance; and $L_{as,bs}$, $L_{bs,cs}$, and $L_{cs,as}$ indicate mutual inductance. Self-inductance is composed of the leakage inductance L_{ls}, constant part L_{0s}, and sinusoidal part L_{2s}. L_{qs} and L_{ds} can be defined as follows:

$$\begin{cases} L_{qs} = [2L_{ls} + 3(L_{0s} + L_{2s})]/2 \\ L_{ds} = [2L_{ls} + 3(L_{0s} - L_{2s})]/2 \end{cases} \tag{5}$$

III. MANUAL MEASUREMENT USING LCR METER

In the conventional manual method for measuring motor inductance, any two phases are connected to the LCR meter, whereas the third phase is left open. Fig. 2 depicts an example in which the line inductance between phases a and b versus the rotor position is first measured. Subsequently, L_{qs} and L_{ds} are deduced from these measurements.

After the rearranging the terms in (1), the line voltage between phases a and b can be expressed as

$$v_{ab} = r_s i_{ab} + L_{ab} p i_{ab} \tag{6}$$

where

$$L_{ab} = 2L_{ls} + 3L_{0s} - 3L_{2s}\cos(2\theta_r - 2\pi/3) \tag{7}$$

After the application of this setup to phases b–c and c–a, the line voltages can be expressed as follows:

$$\begin{cases} v_{ab} = 2r_s i_{ab} + L_{ab} p i_{ab} \\ v_{bc} = 2r_s i_{bc} + L_{bc} p i_{bc} \\ v_{ca} = 2r_s i_{ca} + L_{ca} p i_{ca} \end{cases} \tag{8}$$

where

$$\begin{cases} L_{ab} = 2L_{ls} + 3L_{0s} - 3L_{2s}\cos(2\theta_r - 2\pi/3) \\ L_{bc} = 2L_{ls} + 3L_{0s} - 3L_{2s}\cos(2\theta_r) \\ L_{ca} = 2L_{ls} + 3L_{0s} - 3L_{2s}\cos(2\theta_r + 2\pi/3) \end{cases} \tag{9}$$

According to (9), $\max L_{ab} = \max L_{bc} = \max L_{ca} = 2L_{qs}$ and $\min L_{ab} = \min L_{bc} = \min L_{ca} = 2L_{ds}$. Therefore, the inductance can be obtained by measuring the inductance versus rotor position for at least 180 electrical degrees. Next, half of the maximum line-to-line inductance is L_{qs} and half of the minimum line-to-line inductance is L_{ds}. The aforementioned method requires the measurement of inductance for various rotor positions, which can be improved using a simple linear algebraic algorithm. Algebraically manipulating the trigonometric functions in (9) yields

$$\begin{cases} L_{ab} = 2L_{ls} + 3L_{0s} - \frac{3}{2}L_{2s}\cos(2\theta_r) - \frac{3\sqrt{3}}{2}L_{2s}\sin(2\theta_r) \\ L_{bc} = 2L_{ls} + 3L_{0s} - 3L_{2s}\cos(2\theta_r) \\ L_{ca} = 2L_{ls} + 3L_{0s} - \frac{3}{2}L_{2s}\cos(2\theta_r) + \frac{3\sqrt{3}}{2}L_{2s}\sin(2\theta_r) \end{cases} \tag{10}$$

Let $L_x = L_{2s}\cos(2\theta_r)$, $L_y = L_{2s}\sin(2\theta_r)$, and let $L_z = 2L_{ls} + 3L_{0s}$; (10) can then be rewritten as follows:

$$M \begin{bmatrix} L_x \\ L_y \\ L_z \end{bmatrix} = \begin{bmatrix} L_{ab} \\ L_{bc} \\ L_{ca} \end{bmatrix} \tag{11}$$

and

$$\begin{bmatrix} L_x \\ L_y \\ L_z \end{bmatrix} = M^{-1} \begin{bmatrix} L_{ab} \\ L_{bc} \\ L_{ca} \end{bmatrix} \tag{12}$$

where $M = \begin{bmatrix} \frac{3}{2} & -\frac{3\sqrt{3}}{2} & 1 \\ -3 & 0 & 1 \\ \frac{3}{2} & \frac{3\sqrt{3}}{2} & 1 \end{bmatrix}$. In addition, L_{qs} and L_{ds} can be expressed as follows:

$$\begin{cases} L_{qs} = \dfrac{L_z + 3\sqrt{L_x^2 + L_y^2}}{2} \\ L_{ds} = \dfrac{L_z - 3\sqrt{L_x^2 + L_y^2}}{2} \end{cases} \tag{13}$$

Substituting (12) into (13) enables the calculation of the phase inductance from the line inductance as follows:

$$\begin{cases} L_{temp} = \sqrt{L_{ab}^2 + L_{bc}^2 + L_{ca}^2 - L_{ab}L_{bc} - L_{bc}L_{ca} - L_{ab}L_{ca}} \\ L_{qs} = \dfrac{L_{ab} + L_{bc} + L_{ca}}{6} + \dfrac{L_{temp}}{3} \\ L_{ds} = \dfrac{L_{ab} + L_{bc} + L_{ca}}{6} - \dfrac{L_{temp}}{3} \end{cases} \tag{14}$$

The inductance measurement procedure is based on (14). First, the line inductances L_{ab}, L_{bc}, and L_{ca} are measured using the LCR meter. Then, L_{qs} and L_{ds} are calculated using (14). Compared with the methods described in [4]–[6], the proposed method does not require knowledge of the rotor position, the dc source, or rotor alignment. Thus, the proposed method is a simple and time-efficient method for manually

measuring inductance. Because the common LCR provides a small current, the inductance measured using the LCR can be viewed as light load inductance. Consequently, this inductance can be regarded as the maximum inductance for current controller design. In addition to the inductance, the rotor position can be calculated from the definition of L_x and L_y as follows:

$$\tan(2\theta_r) = \frac{L_y}{L_x} \tag{15}$$

However, the aforementioned calculated position requires a polarity check, which can be performed using the method presented in [13].

IV. LLVI WITH SENSORLESS DRIVE

The LLVI method energizes only two phases at a time, whereas the third phase remains floating. This method is similar to the scheme for driving brushless DC motors, where both the inductance and rotor position are measured offline.

Neglecting the resistance drop and assuming that the voltage error caused by the nonlinear effect, such as dead time, has been compensated for, (8) can be expressed in difference form as follows:

$$\begin{cases} T_p v_{ab\_act} = L_{ab}\Delta i_{ab} \\ T_p v_{bc\_act} = L_{bc}\Delta i_{bc} \\ T_p v_{ca\_act} = L_{ca}\Delta i_{ca} \end{cases} \tag{16}$$

where T_p is the time to apply the voltage pulse; v_{ab_act}, v_{bc_act}, and v_{ca_act} indicate the actual voltages applied to the motor; and Δi_{ab}, Δi_{bc}, and Δi_{ca} indicate the difference currents. Under the assumption that $\Delta i_{ab}\Delta i_{bc}\Delta i_{ca} \neq 0$, replacing the inductance in (11) with that in (16) yields

$$M \begin{bmatrix} L_x \\ L_y \\ L_z \end{bmatrix} = T_p \begin{bmatrix} \frac{v_{ab\_act}}{\Delta i_{ab}} \\ \frac{v_{bc\_act}}{\Delta i_{bc}} \\ \frac{v_{ca\_act}}{\Delta i_{ca}} \end{bmatrix} \tag{17}$$

Because (11) and (17) have the same form, the inductance and rotor position can be calculated using similar procedures, except for the line voltage and difference current used in the calculations. To ensure measurement accuracy, multiple voltage vectors are applied to the motor and the least-squares algorithm is used in the calculations.

Assuming that n group voltage vectors are injected into the motor, where $n \geq 1$, (17) can be expanded as follows:

$$A_{LL} \begin{bmatrix} L_x \\ L_y \\ L_z \end{bmatrix} = y_{LL} \tag{18}$$

where

$$A_{LL}^T = \begin{bmatrix} \frac{3}{2} & -3 & \frac{3}{2} & \cdots & \frac{3}{2} & -3 & \frac{3}{2} \\ -\frac{3\sqrt{3}}{2} & 0 & \frac{3\sqrt{3}}{2} & \cdots & -\frac{3\sqrt{3}}{2} & 0 & \frac{3\sqrt{3}}{2} \\ 1 & 1 & 1 & \cdots & 1 & 1 & 1 \end{bmatrix}$$

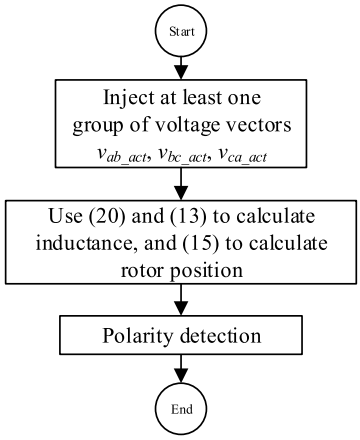

FIGURE 3. Flowchart for the line-to-line voltage injection (LLVI) measurement method.

and

$$y_{LL}^T = \begin{bmatrix} \frac{v_{ab\_act,1}}{\Delta i_{ab,1}} & \frac{v_{bc\_act,1}}{\Delta i_{bc,1}} & \frac{v_{ca\_act,1}}{\Delta i_{ca,1}} & \cdots & \frac{v_{ab\_act,n}}{\Delta i_{ab,n}} & \frac{v_{bc\_act,n}}{\Delta i_{bc,n}} & \frac{v_{ca\_act,n}}{\Delta i_{ca,n}} \end{bmatrix}$$

where $v_{ab\_act,k}$, $v_{bc\_act,k}$, and $v_{ca\_act,k}$ are the kth group voltage vectors; $\Delta i_{ab,k}$, $\Delta i_{bc,k}$, and $\Delta i_{ca,k}$ are the kth group difference currents; and k ranges from 1 to n. Thus, the following expression is obtained:

$$A_{LL}^T A_{LL} = \frac{27}{2} n \begin{bmatrix} 1 & 0 & 0 \\ 0 & 1 & 0 \\ 0 & 0 & \frac{2}{9} \end{bmatrix} \tag{19}$$

Because the determinant of $A_{LL}^T A_{LL}$ is nonzero, the least-squares solution of (18) is expressed as follows:

$$\begin{bmatrix} L_x \\ L_y \\ L_z \end{bmatrix} = (A_{LL}^T A_{LL})^{-1} A_{LL}^T y_{LL} \tag{20}$$

Fig. 3 illustrates the LLVI measurement procedures. At least one voltage group should be applied, and each voltage group contains three voltage vectors: v_{ab_act}, v_{bc_act}, and v_{ca_act}.

Because only two phases are energized to produce a voltage vector, its equivalent circuit is similar to that presented in Fig. 2. The difference currents produced by each voltage group are recorded; subsequently, (20) and (13) are used to evaluate the phase inductance, and (15) is used to evaluate the rotor position. Next, rotor polarity is detected and the measured position is compensated for if necessary. The magnitude and duration of the injected voltages should be sufficiently small to prevent rotor movement.

V. STATOR QD VOLTAGE INJECTION AND RESISTANCE ESTIMATION WITH SENSORLESS DRIVE

The QDVI method involves injecting at least two voltage vectors at the stator qd axis and then calculating the phase inductance and rotor position by using the difference currents and a least-squares algorithm. Assuming that the rotor is at position θ_r and neglecting the speed terms, (1) can be

transformed to be in terms of the stator qd frame as follows:

$$\begin{cases} v^s_{qs} = r_s i^s_{qs} + L_{x\_qd} p i^s_{qs} - L_{y\_qd} p i^s_{ds} + L_{z\_qd} p i^s_{qs} \\ v^s_{ds} = r_s i^s_{ds} - L_{x\_qd} p i^s_{ds} - L_{y\_qd} p i^s_{qs} + L_{z\_qd} p i^s_{ds} \end{cases} \tag{21}$$

where v^s_{qs}, v^s_{ds} are the q and d axis voltages, i^s_{qs}, i^s_{ds} are the q and d axis currents, $L_{x\_qd} = 0.5(L_{qs} - L_{ds})\cos(2\theta_r)$, $L_{y\_qd} = 0.5(L_{qs} - L_{ds})\sin(2\theta_r)$, and $L_{z\_qd} = 0.5(L_{qs} + L_{ds})$. Then, neglecting the resistance drop and other voltage errors, (21) can be expressed in the difference form as follows:

$$\begin{cases} T_p v^s_{qs\_act} = L_{x\_qd} \Delta i^s_{qs} - L_{y\_qd} \Delta i^s_{ds} + L_{z\_qd} \Delta i^s_{qs} \\ T_p v^s_{ds\_act} = -L_{x\_qd} \Delta i^s_{ds} - L_{y\_qd} \Delta i^s_{qs} + L_{z\_qd} \Delta i^s_{ds} \end{cases} \tag{22}$$

where $v^s_{qs\_act}$, $v^s_{ds\_act}$ are the voltages applied to the motor and Δi^s_{qs}, Δi^s_{ds} are the difference currents. Equation (22) describes the relation between the voltage and current vectors. Because (22) contains three unknown variables, the solution is not unique. However, if n stator voltage vectors are applied, where $n \geq 2$, the following expression can be obtained:

$$A_{qd} \begin{bmatrix} L_{x\_qd} \\ L_{y\_qd} \\ L_{z\_qd} \end{bmatrix} = y_{qd} \tag{23}$$

where

$$A^T_{qd} = \begin{bmatrix} \Delta i^s_{qs,1} & -\Delta i^s_{ds,1} & \cdots & \Delta i^s_{qs,n} & -\Delta i^s_{ds,n} \\ -\Delta i^s_{ds,1} & -\Delta i^s_{qs,1} & \cdots & -\Delta i^s_{ds,n} & -\Delta i^s_{qs,n} \\ \Delta i^s_{qs,1} & \Delta i^s_{ds,1} & \cdots & \Delta i^s_{qs,n} & \Delta i^s_{ds,n} \end{bmatrix},$$

$y^T_{qd} = T_p \left[v^s_{qs\_act,1}\ v^s_{ds\_act,1} \cdots v^s_{qs\_act,n}\ v^s_{ds\_act,n} \right]$. Here, $(v^s_{qs\_act,k}, v^s_{ds\_act,k})$ is the kth injection voltage vector, $(\Delta i^s_{qs,k}, \Delta i^s_{ds,k})$ is the kth difference current vector induced by the kth voltage vector, and k ranges from 1 to n. At least two current vectors with a nonzero vector cross-product are required; thus, the least-squares solution of (23) exists as (18) [31]. Therefore, we obtain the following expression:

$$\begin{bmatrix} L_{x\_qd} \\ L_{y\_qd} \\ L_{z\_qd} \end{bmatrix} = (A^T_{qd} A_{qd})^{-1} A^T_{qd} y_{qd} \tag{24}$$

Consequently, the phase inductance can be calculated as

$$\begin{cases} L_{qs} = L_{z\_qd} + \sqrt{L^2_{x\_qd} + L^2_{y\_qd}} \\ L_{ds} = L_{z\_qd} - \sqrt{L^2_{x\_qd} + L^2_{y\_qd}} \end{cases} \tag{25}$$

and the rotor position can be expressed as

$$\tan(2\theta_r) = \frac{L_{y\_qd}}{L_{x\_qd}} \tag{26}$$

Fig. 4 illustrates the procedures for measuring the inductance and rotor position by using the aforementioned method. At least two voltage vectors with different orientations should be injected, each of which contains a q and a d axis voltage component. First, the difference currents are recorded, and then, (24) and (25) are used to calculate the inductance and (26) is used to calculate the rotor position.

The phase resistance can be estimated after the inductance and initial position have been determined. The resistance is measured by applying two consecutive dc voltages to the d axis of the positive rotor frame [11]. Because the inductance voltage drop is nearly zero at steady state, the phase resistance is identified as

$$r_s = \frac{v^r_{ds\_act,1} - v^r_{ds\_act,2}}{i^r_{ds\_act,1} - i^r_{ds\_act,2}} \tag{27}$$

where $(v^r_{ds\_act,1}, v^r_{ds\_act,1})$ and $(i^r_{ds\_act,1}, i^r_{ds\_act,1})$ are the applied voltages and the corresponding measured currents.

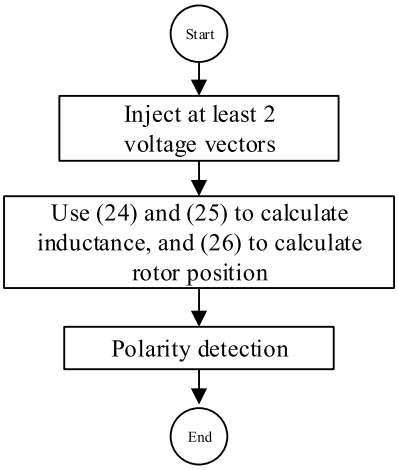

FIGURE 4. Flowchart for the QD voltage injection (QDVI) measurement method.

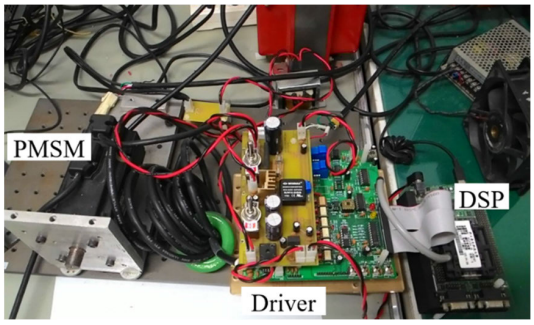

FIGURE 5. Experimental system.

VI. EXPERIMENTAL RESULTS

An IPMSM and an SPMSM were used for experimentally verifying the proposed methods. Fig. 5 illustrates the experimental system. The inductance and initial rotor position estimation algorithms were implemented using a Texas Instruments TMS320F28335 digital signal processor at an execution rate of 10 kHz. A load motor provided the external load to the test motor. Table 1 lists the machines' parameters and the nominal motor inductance. These inductances were measured using the conventional line-to-line method, described in Section 3, and the nominal inductance was used as a reference for comparison with the inductance measured using the other methods.

TABLE 1. Parameters of the machines used for experimental verification.

Parameter	Quantity	Units [a]
r_s of IPMSM	1.25	ohm
L_{qs} of IPMSM	5.94	mH
L_{ds} of IPMSM	3.97	mH
r_s of SPMSM	2.3	ohm
L_{qs} of SPMSM	6.47	mH
L_{ds} of SPMSM	5.83	mH

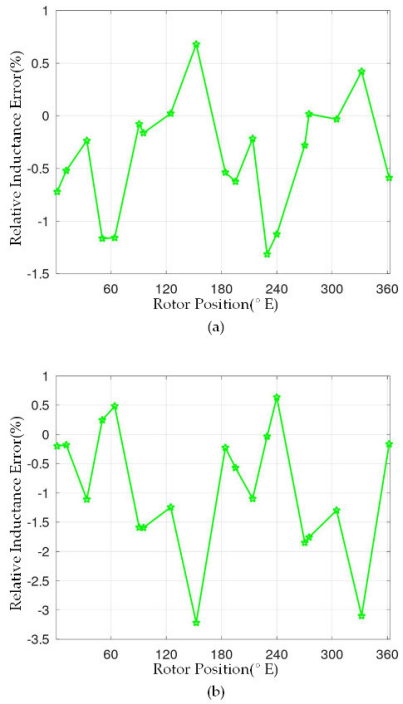

FIGURE 6. Measured relative inductance error versus rotor position for the IPMSM with the improved manual measurement method and LCR meter; (a) L_{qs} and (b) L_{ds}.

A. RESULTS FOR IMPROVED MANUAL METHOD WITH LCR METER

Figs. 6(a) and (b) illustrate the relative errors of L_{qs} and L_{ds}, respectively, of IPMSM for various rotor positions measured using the improved manual measurement method described in Section 3. Figs. 7(a) and (b) depict the relative errors of L_{qs} and L_{ds}, respectively, of SPMSM for various rotor positions measured using the same method. The measured inductances were relatively stable regardless of the rotor position, and all measured inductance errors were within 5% for both machines. The measurement was performed within a few minutes, because rotor position alignment was not required.

B. RESULTS OF LLVI WITH SENSORLESS DRIVER

Figs. 8–11 illustrate the results of the relative inductance error and initial rotor position estimated with LLVI using a sensorless driver. For comparison, two sets of experiments were conducted: (1) experiments with the injection of six voltage vectors (i.e., v_{ab}, v_{bc}, and v_{ca} and $-v_{ab}$, $-v_{bc}$, and $-v_{ca}$) and (2) experiments with the injection of three voltage

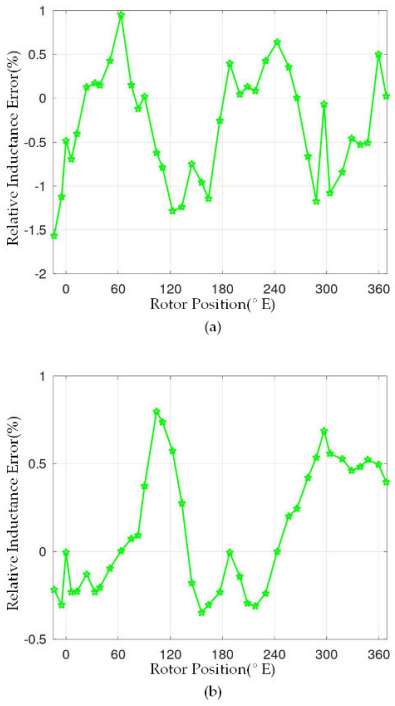

FIGURE 7. Measured relative inductance error versus rotor position for the SPMSM with the improved manual measurement method and LCR meter; (a) L_{qs} and (b) L_{ds}.

vectors (i.e., v_{ab}, v_{bc}, and v_{ca}). The injection time required for each voltage vector was 100 μs (i.e., one PWM sampling time), and the average magnitudes of the injection voltages were 120 and 165 V for IPMSM and SPMSM, respectively. Because the pulse width was very short, the machine was essentially not saturated and the identified inductance was unsaturated inductance.

Figs. 8(a) and (b) illustrate the relative errors of L_{qs} and L_{ds}, respectively, for IPMSM, and Figs. 9(a) and (b) illustrate those of L_{qs} and L_{ds} for SPMSM. The results obtained for six-vector injection were slightly superior to those obtained for three-vector injection. However, the measured errors of L_{qs} were less than 11% for both machines. Moreover, the L_{ds} of SPMSM exhibited the maximum error, which was approximately 16%.

Figs. 10(a) and (b) depict the measured rotor positions for IPMSM and SPMSM, respectively, and Figs. 11(a) and (b) depict their position errors. Both test machines had an encoder mounted on the shaft, whose position was treated as the reference position in the experimental results. For six-vector injections, the position errors were less than 5° for IPMSM and less than 12° for SPMSM. For three-vector injections, the position errors were less than 8° for IPMSM and more than 80° for SPMSM. Therefore, the results obtained for six-vector injections were considerably better than those obtained for three-vector injections. Moreover, the injection of only three voltage vectors was insufficient to estimate the rotor position for SPMSM. Table 2 summarizes the experimental results obtained for the LLVI method.

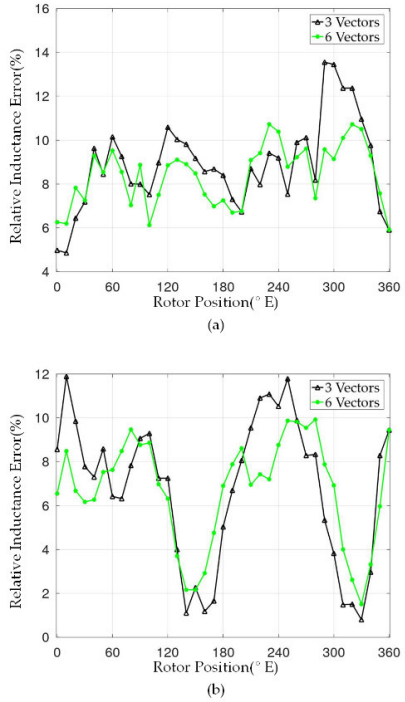

FIGURE 8. Measured relative inductance error versus rotor position for the IPMSM with LLVI; (a) L_{qs} and (b) L_{ds}.

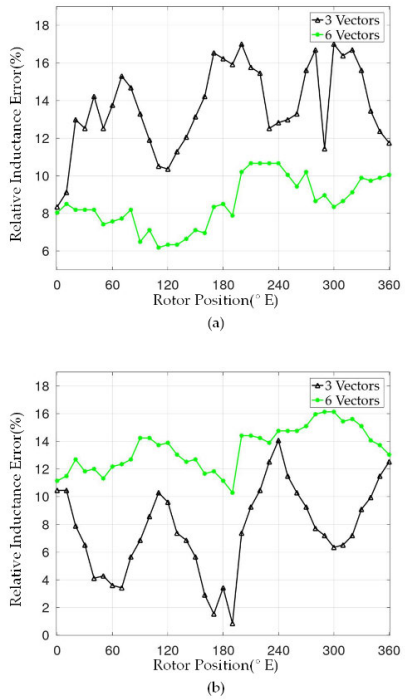

FIGURE 9. Measured relative inductance error versus rotor position for the SPMSM with LLVI; (a) L_{qs} and (b) L_{ds}.

C. RESULTS OF QDVI WITH SENSORLESS DRIVER

Figs. 12–15 illustrate the results of relative inductance error and initial rotor position estimated with QDVI and a sensorless driver. Six linearly independent injection voltage vectors were used in the experiments (i.e., 0°, 60°, 120°, 180°, 240°, and 300°) in the stator frame. The average magnitudes of the injected voltage for IPMSM and SPMSM were 70 and 110 V, respectively. For comparison, three sets of experiments were conducted: (1) experiments with injection with two vectors (180° and 300°), (2) experiments with injection with three vectors (60°, 180°, and 300°), and (3) experiments with injection with all six vectors.

Figs. 12(a) and (b), respectively, display the relative errors of L_{qs} and L_{ds} for IPMSM, and Figs. 13(a) and (b) depict those for SPMSM. The inductance error decreased as the number of injection vectors was increased. The measured errors of L_{qs} were less than 9% for both machines with six-vector injections. They were also less than 9% for IPMSM with three-vector injections but approximately 13% for SPMSM

TABLE 2. Summary of the experimental results for LLVI.

Measurement Error	Quantity	Units
L_{ds} Error(SPM-3 Vectors)	14	%
L_{ds} Error(SPM-6 Vectors)	16	%
L_{qs} Error(SPM-3 Vectors)	17	%
L_{qs} Error(SPM-6 Vectors)	11	%
Position Error(SPM-3 Vectors)	80	°E
Position Error(SPM-6 Vectors)	11	°E
L_{ds} Error(IPM-3 Vectors)	12	%
L_{ds} Error(IPM-6 Vectors)	10	%
L_{qs} Error(IPM-3 Vectors)	13.5	%
L_{qs} Error(IPM-6 Vectors)	11	%
Position Error(IPM-3 Vectors)	8	°E
Position Error(IPM-6 Vectors)	4	°E

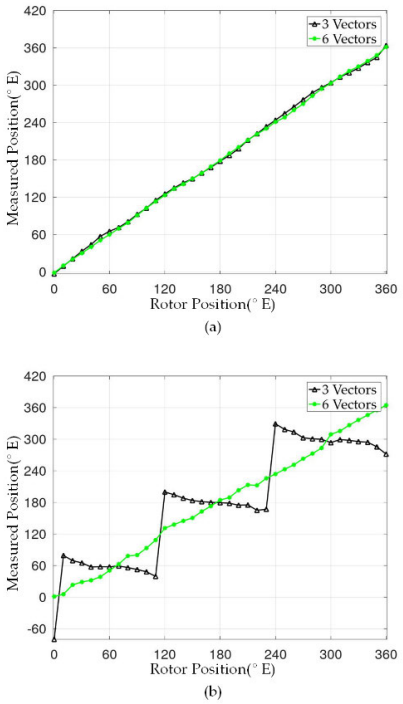

FIGURE 10. Measured position versus rotor position with LLVI; (a) IPMSM and (b) SPMSM.

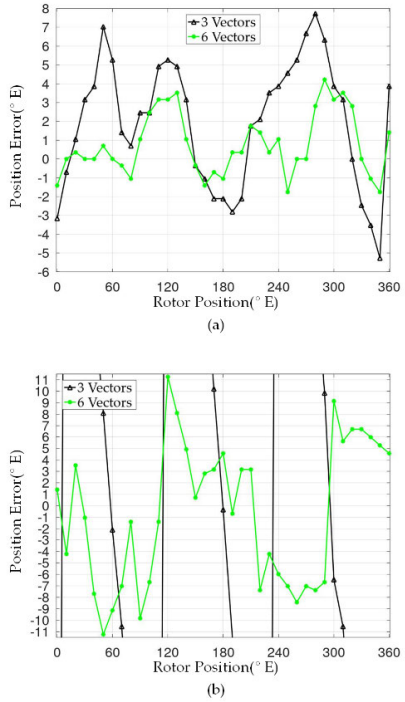

FIGURE 11. Position error versus rotor position with LLVI; (a) IPMSM and (b) SPMSM.

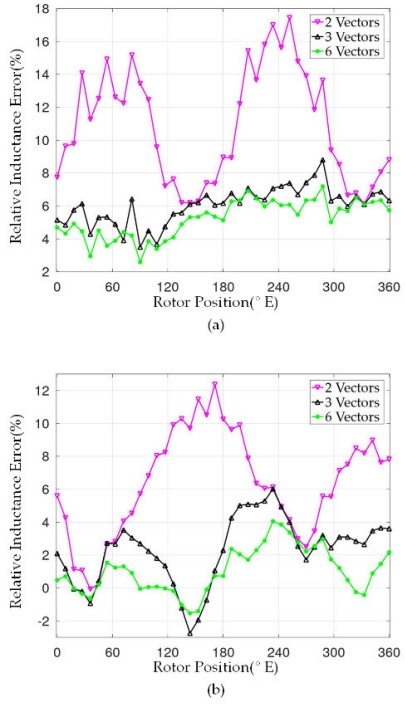

FIGURE 12. Measured relative inductance error versus rotor position for the IPMSM with QDVI; (a) L_{qs} and (b) L_{ds}.

with three-vector injections. However, for two-vector injections, the measured errors increased considerably to approximately 17% for IPMSM and 23% for SPMSM.

Figs. 14(a) and (b) illustrate the measured rotor positions for IPMSM and SPMSM, respectively, and

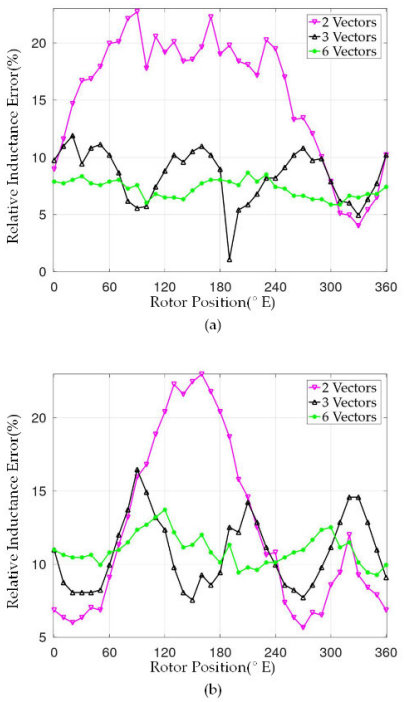

FIGURE 13. Measured relative inductance error versus rotor position for the SPMSM with QDVI; (a) L_{qs} and (b) L_{ds}.

Figs. 15(a) and (b) present their corresponding position errors. The position errors for IPMSM were less than 4° for six- and three-vector injections and less than 7° for two-vector injection. By contrast, the position errors for SPMSM were approximately 10° for six-vector injection and more than 60° for three- and two-vector injections. These results indicate that the accuracy of the estimated position is linearly proportional to the number of voltage vectors injected. Moreover, the proposed method is more suitable for IPMSM; the estimated position is sufficiently accurate for most sensorless control applications. However, only rough positions can be obtained for SPMSM, even with six-vector injection, and the error is too large for most sensorless control applications. Table 3 summarizes the experimental results obtained using the QDVI method.

D. DYNAMIC REPONSES OF ESTIMATION PROCESS

Fig. 16 presents the dynamic responses of the stationary frame currents and the resistance estimated using QDVI and IPMSM at 30°E. First, six voltage vectors were injected to estimate the phase inductance and rotor position. Then, the polarity of the estimated position was determined using four larger voltage pulses [13]. The magnitude and duration of the pulses for polarity check were 90 V and 100 μs for IPMSM, respectively, and 120 V and 100 μs for SPMSM, respectively. Finally, the phase resistance was identified with two voltage vectors of longer durations. The first voltage vector contained 1.69 V for IPMSM and 3.11 V for SPMSM, and the second voltage vector contained 1 V for IPMSM and 1.84 V for

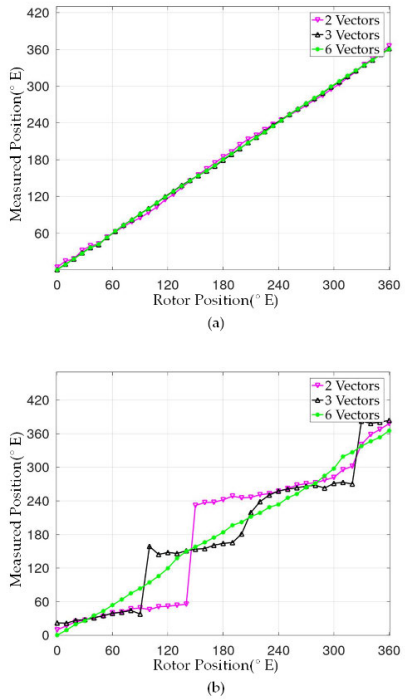

FIGURE 14. Measured position versus rotor position with QDVI; (a) IPMSM and (b) SPMSM.

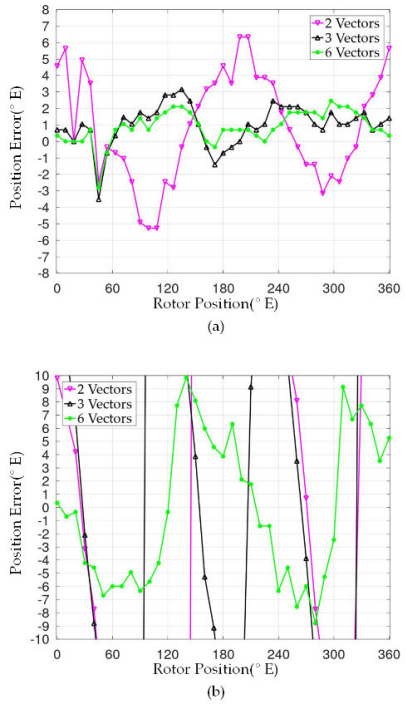

FIGURE 15. Position error versus rotor position with QDVI; (a) IPMSM and (b) SPMSM.

SPMSM. The duration for these voltage pulses was 15 ms. The total elapsed time for the estimation process was approximately 55 ms; the estimation of the inductance, position, and polarity took less than 25 ms. Fig. 17 displays the dynamic

TABLE 3. Summary of the experimental results for QDVI.

Measurement Error	Quantity	Units
L_{ds} Error(SPM-2 Vectors)	23	%
L_{ds} Error(SPM-3 Vectors)	16	%
L_{ds} Error(SPM-6 Vectors)	13	%
L_{qs} Error(SPM-2 Vectors)	23	%
L_{qs} Error(SPM-3 Vectors)	12	%
L_{qs} Error(SPM-6 Vectors)	9	%
Position Error(SPM-2 Vectors)	80	°E
Position Error(SPM-3 Vectors)	60	°E
Position Error(SPM-6 Vectors)	10	°E
L_{ds} Error(IPM-2 Vectors)	12	%
L_{ds} Error(IPM-3 Vectors)	6	%
L_{ds} Error(IPM-6 Vectors)	4	%
L_{qs} Error(IPM-2 Vectors)	17	%
L_{qs} Error(IPM-3 Vectors)	9	%
L_{qs} Error(IPM-6 Vectors)	7	%
Position Error(IPM-2 Vectors)	6	°E
Position Error(IPM-3 Vectors)	4	°E
Position Error(IPM-6 Vectors)	3	°E

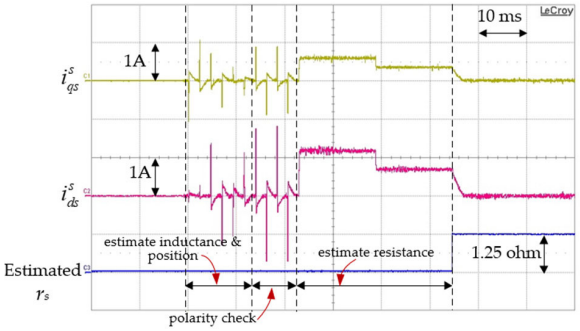

FIGURE 16. Dynamic response of QDVI estimation process for IPMSM at 30°E.

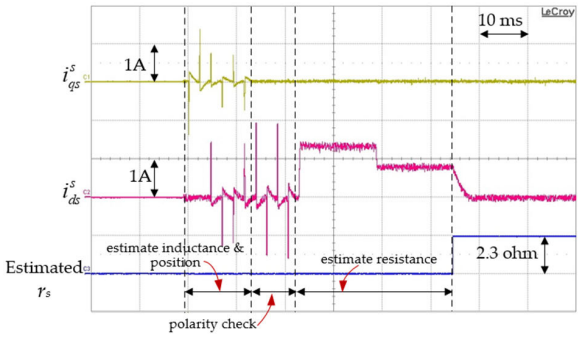

FIGURE 17. Dynamic response of QDVI estimation process for SPMSM at 0°E.

responses of the currents and the estimated resistance during the estimation process with QDVI for SPMSM at 0°E. The total elapsed time was approximately 55 ms. Because the rotor was located at 0°E, no voltage was applied at the q axis when estimating the phase resistance.

E. RESULTS FOR PHASE RESISTANCE ESTIMATION

Figs. 18(a) and (b) present the measured phase resistance error versus rotor position for IPMSM and SPMSM, respectively. The maximum relative resistance error was 12% for

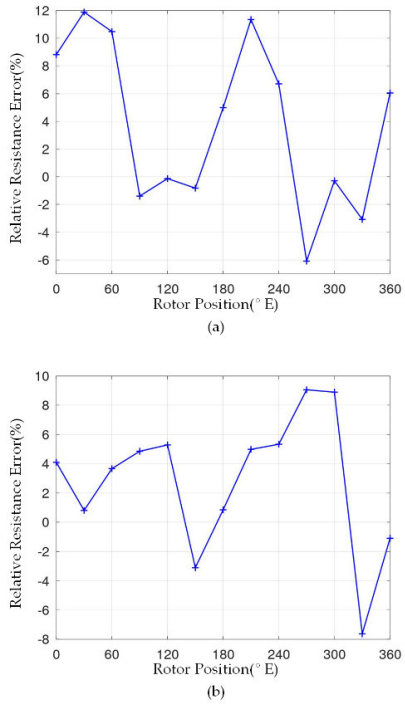

FIGURE 18. Measured relative resistance error versus rotor position; (a) IPMSM and (b) SPMSM.

IPMSM and 9% for SPMSM. Thus, the accuracy was sufficient for current controller design.

F. RESULTS FOR D-AXIS CURRENT CONTROL RESPONSE

Fig. 19 displays the current control response of IPMSM at the estimated d axis. A common constant PI current controller was used as the controller. Pole zero cancellation with the estimated parameters was used for designing the PI gain. Because the parameters in this experiment varied little, the current response was satisfactory.

G. COMPARISON WITH EXISTING METHODS

The main principle of standstill initial position detection for PMSMs is the use of the saliency effect. Typically, a large saliency ratio results in better position detection accuracy. The saliency ratio of the tested IPMSMs in [15]–[20] ranged from 1.33 [18] to 3.5 [17], and the measured position error ranged from 3°E [18], [20] to 6°E [15], [16]. The saliency ratio of the IPMSM used in this study was 1.5. The position errors measured using the QDVI and LLVI methods were 3°E and 4°E, respectively. However, in [19], the saliency ratio of the tested SPMSM was 1.11 and the measured position error was 30°E. The saliency ratio of the SPMSM used in this study was also 1.11. However, the measured position errors with the QDVI and LLVI methods were only 10°E and 11°E, respectively.

The initial position detection time demonstrated in the existing methods was approximately 40 ms [15], [17–19]. However, as shown in Figs. 16 and 17, the initial position detection time with QDVI was less than 25 ms. Thus,

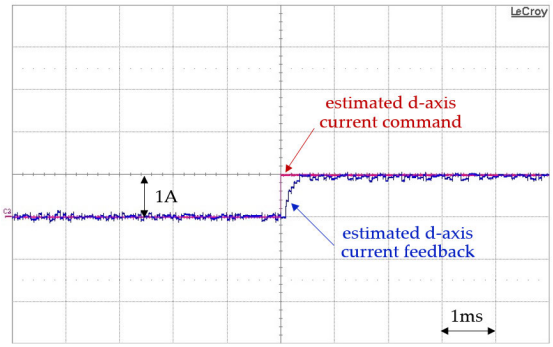

FIGURE 19. Estimated d-axis current PI control of IPMSM with estimated inductance and resistance.

compared with the existing methods [15]–[20], the proposed method is more accurate and faster; moreover, the phase inductance can be estimated using the same algorithm.

Although the inductance estimated using the proposed methods did not include the saturation and crosscoupling effects, the proposed methods can be used to design the current controllers. Fig. 19 depicts a typical current response in which the controller is tuned with the estimated phase inductance.

VII. CONCLUSION

This paper proposes two offline inductance measurement methods, LLVI and stator QDVI, for sensorless PMSM drives, both of which are based on voltage vector injection and use the least-squares algorithms. LLVI energizes only two phases at a time, whereas the third phase remains floating. Stator QDVI outputs voltage vectors in the stator frame. Although both methods are based on the same principle, they differ in how the inverter stage is controlled. A distinct feature of these methods is that both the inductance and rotor position can be estimated simultaneously by using the same algorithm.

The LLVI results indicated that the inductance measurements were reasonably accurate for both machines; all errors were less than 16%, but the injection of more vectors yielded superior results. In addition, the measured rotor positions were reasonably accurate for six-vector injections, at less than 10° for both machines. Similarly, the injection of more vectors yielded superior results. However, for SPMSM, the application of six or more vectors was necessary to obtain reasonably accurate position estimates. A similar trend was observed for QDVI, although the errors were generally smaller than those obtained for LLVI. With six-vector injections, the measured inductance errors were less than 13% for both machines. However, they increased to 17% and 23% for IPMSM and SPMSM, respectively, for two-vector injection. This is similar to the LLVI findings, where the injection of more vectors yielded superior results.

The errors in position estimation were less than 4° for IPMSM for six- and three-vector injections and less than 6° for two-vector injection. By contrast, the errors for SPMSM were approximately 10° for six-vector injections and more than 60° for three- and two-vector injections.

Again, the results indicate that the accuracy of the position estimates is linearly proportional to the number of voltage vectors injected. The measured resistance error was less than 12% for IPMSM and less than 9% for SPMSM. The application of a least-squares algorithm in the estimations enabled reasonable accuracy to be achieved by the proposed methods for measuring the phase inductance and initial rotor position under the application of sufficient voltage vectors.

REFERENCES

[1] S. Kim and S.-K. Sul, "Sensorless control of AC motor—Where are we now?" in *Proc. Int. Conf. Elect. Mach. Syst.*, Aug. 2011, pp. 1–6.

[2] Z. Chen, M. Tomita, S. Doki, and S. Okuma, "An extended electromotive force model for sensorless control of interior permanent-magnet synchronous motors," *IEEE Trans. Ind. Electron.*, vol. 50, no. 2, pp. 288–295, Apr. 2003.

[3] Y.-D. Yoon, S.-K. Sul, S. Morimoto, and K. Ide, "High-bandwidth sensorless algorithm for AC machines based on square-wave-type voltage injection," *IEEE Trans. Ind. Appl.*, vol. 47, no. 3, pp. 1361–1370, May/Jun. 2011.

[4] Y. Gao, R. Qu, and Y. Liu, "An improved AC standstill method for inductance measurement of interior permanent magnet synchronous motors," in *Proc. Int. Conf. Electr. Mach. Syst.*, Oct. 2013, pp. 927–931.

[5] V. Bobek, *PMSM Electrical Parameters Measurement*, Freescale Semiconductor document AN4680, Freescale Semiconductor Ltd, Austin, TX, USA, 2013.

[6] Y. Gao, R. Qu, Y. Chen, J. Li, and W. Xu, "Review of off-line synchronous inductance measurement method for permanent magnet synchronous machines," in *Proc. IEEE Conf. Expo Transp. Electrific. Asia–Pacific*, Aug. 2014, pp. 1–6.

[7] S. A. Odhano, R. Bojoi, Ş. G. Roşu, and A. Tenconi, "Identification of the magnetic model of permanent-magnet synchronous machines using DC-biased low-frequency AC signal injection," *IEEE Trans. Ind. Appl.*, vol. 51, no. 4, pp. 3208–3215, Jul./Aug. 2015.

[8] K. Liu and Z. Q. Zhu, "Determination of electrical parameters of PMSM drive system at standstill," in *Proc. IEEE Vehicle Power Propuls. Conf.*, Oct. 2016, pp. 1–6.

[9] A. Cavagnino, G. Pellegrino, S. Vaschetto, and E. B. Agamloh, "Contribution to offline measurements of PMSM and SyRM inductances," *IEEE Trans. Ind. Appl.*, vol. 55, no. 1, pp. 407–416, Jan./Feb. 2019.

[10] G. Li, Z. Wu, S. Han, F. Jiang, T. Yang, and G. Wang, "Modified AC standstill method for PMSM $d-q$ axis inductances measurement," *IET Sci., Meas. Technol.*, vol. 14, no. 4, pp. 430–434, Jun. 2020.

[11] S.-M. Yang and K.-W. Lin, "Automatic control loop tuning for permanent-magnet AC servo motor drives," *IEEE Trans. Ind. Electron.*, vol. 63, no. 3, pp. 1499–1506, Mar. 2016.

[12] D. Raca, M. C. Harke, and R. D. Lorenz, "Robust magnet polarity estimation for initialization of PM synchronous machines with near zero saliency," in *Proc. Conf. Rec. IEEE Ind. Appl. Conf. 41st IAS Annu. Meeting*, Oct. 2006, pp. 481–487.

[13] S.-C. Yang, S.-M. Yang, and J.-H. Hu, "Robust initial position estimation of permanent magnet machine with low saliency ratio," *IEEE Access*, vol. 5, pp. 2685–2695, Feb. 2017.

[14] J. Holtz, "Acquisition of position error and magnet polarity for sensorless control of PM synchronous machines," *IEEE Trans. Ind. Appl.*, vol. 44, no. 4, pp. 1172–1180, Jul./Aug. 2008.

[15] X. Wu, S. Huang, X. Liu, K. Lu, J. Gao, and J. Zheng, "Design of position estimation strategy of sensorless interior PMSM at standstill using minimum voltage vector injection method," *IEEE Trans. Magn.*, vol. 53, no. 11, pp. 1–4, Nov. 2017.

[16] X. Wu, S. Huang, P. Liu, T. Wu, Y. He, X. Zhang, K. Chen, and Q. Wu, "A reliable initial rotor position estimation method for sensorless control of interior permanent magnet synchronous motors," *ISA Trans.*, vol. 97, pp. 116–129, Feb. 2020.

[17] X. Zhang, H. Li, S. Yang, and M. Ma, "Improved initial rotor position estimation for PMSM drives based on HF pulsating voltage signal injection," *IEEE Trans. Ind. Electron.*, vol. 65, no. 6, pp. 4702–4713, Jun. 2018.

[18] G. Bi, G. Wang, G. Zhang, N. Zhao, and D. Xu, "Low-noise initial position detection method for sensorless permanent magnet synchronous motor drives," *IEEE Trans. Power Electron.*, vol. 35, no. 12, pp. 13333–13344, Dec. 2020.

[19] Z. Wang, Z. Cao, and Z. He, "Improved fast method of initial rotor position estimation for interior permanent magnet synchronous motor by symmetric pulse voltage injection," *IEEE Access*, vol. 8, pp. 59998–60007, Mar. 2020.

[20] T. Wu, D. Luo, S. Huang, X. Wu, K. Liu, K. Lu, and X. Peng, "A fast estimation of initial rotor position for low-speed free-running IPMSM," *IEEE Trans. Power Electron.*, vol. 35, no. 7, pp. 7664–7673, Jul. 2020.

[21] S. Morimoto, M. Sanada, and Y. Takeda, "Mechanical sensorless drives of IPMSM with online parameter identification," *IEEE Trans. Ind. Appl.*, vol. 42, no. 5, pp. 1241–1248, Sep./Oct. 2006.

[22] J. Liu, M. M. Harbaugh, T. A. Nondahl, P. B. Schmidt, and S. Royak, "Method and apparatus for automatically identifying electrical parameters in a sensor-less PMSM," U.S. Patent 8 228 013 B2, Jul. 24, 2012.

[23] G. Wang, L. Qu, H. Zhan, J. Xu, L. Ding, G. Zhang, and D. Xu, "Self-commissioning of permanent magnet synchronous machine drives at standstill considering inverter nonlinearities," *IEEE Trans. Power Electron.*, vol. 29, no. 12, pp. 6615–6627, Dec. 2014.

[24] X. Fu, H. He, Y. Xu, and X. Fu, "A strongly robust and easy-tuned current controller for PMSM considering parameters variation," *IEEE Access*, vol. 8, pp. 44228–44238, Feb. 2020.

[25] Z.-C. You, C.-H. Huang, and S.-M. Yang, "Online current loop tuning for permanent magnet synchronous servo motor drives with deadbeat current control," *Energies*, vol. 12, no. 18, p. 3555, Sep. 2019.

[26] S. Ichikawa, M. Tomita, S. Doki, and S. Okuma, "Sensorless control of permanent-magnet synchronous motors using online parameter identification based on system identification theory," *IEEE Trans. Ind. Electron.*, vol. 53, no. 2, pp. 363–372, Apr. 2006.

[27] S. J. Underwood and I. Husain, "Online parameter estimation and adaptive control of permanent-magnet synchronous machines," *IEEE Trans. Ind. Electron.*, vol. 57, no. 7, pp. 2435–2443, Jul. 2010.

[28] M. A. Hamida, J. De Leon, A. Glumineau, and R. Boisliveau, "An adaptive interconnected observer for sensorless control of PM synchronous motors with online parameter identification," *IEEE Trans. Ind. Electron.*, vol. 60, no. 2, pp. 739–748, Feb. 2013.

[29] T. Boileau, N. Leboeuf, B. Nahid-Mobarakeh, and F. Meibody-Tabar, "Online identification of PMSM parameters: Parameter identifiability and estimator comparative study," *IEEE Trans. Ind. Appl.*, vol. 47, no. 4, pp. 1944–1957, Jul./Aug. 2011.

[30] P. Krause, O. Wasynczuk, S. D. Sudhoff, and S. Pekarek, "Permanent-magnet AC machines," in *Analysis of Electric Machinery and Drive Systems*, 3rd ed. New York, NY, USA: Wiley, 2013, pp. 122–126.

[31] H. C. Yeh, "Parameter identification for position sensorless controlled permanent magnet synchronous machine," M.S. thesis, Dept. Electr. Eng., Nat. Taipei Univ. Technol., Taipei, Taiwan, 2018.

HAO-CHIEH YEH was born in Pingtung, Taiwan. He received the bachelor's and M.S. degrees in aeronautics and astronautics engineering from National Cheng Kung University, Tainan, Taiwan, in 2004 and 2006, respectively, and the M.S. degree in electrical engineering from the National Taipei University of Technology, Taipei, Taiwan, in 2018. His research interest includes motor drive and control.

SHENG-MING YANG (Member, IEEE) was born in Taiwan. He received the M.S. and Ph.D. degrees from the University of Wisconsin at Madison, in 1985 and 1989, respectively. From 1989 to 1992, he was a Development Engineer with Unico Inc. From 1992 to 1995, he was a Principal Engineer with A. O. Smith Corporate Technology Center, Milwaukee. In 1995, he was a Professor with the Department of Mechanical and Electro-Mechanical Engineering, Tamkang University, Taiwan. Since 2007, he has been with the Department of Electrical Engineering, National Taipei University of Technology, Taiwan. His research interest includes ac and dc motor drives and control.